Spectrum of a one-atom laser in photonic crystals

Lucia Florescu
Jet Propulsion Laboratory, California Institute of Technology, Mail Stop 126-347, 4800 Oak Grove Drive, Pasadena, California 91109-8099, USA

(Received 29 September 2006; published 26 December 2006)

The emission spectrum of a single-emitter laser in a photonic crystal is presented. We consider a coherently pumped two-level emitter strongly coupled to a high-quality microcavity engineered within a photonic crystal. We show that the cavity spectrum consists of both elastic and inelastic components, for which we derive analytical expressions. Our study reveals enhanced, spectrally narrower emission resulting from the radiation reservoir of the photonic crystal. The cavity field spectral characteristics are fundamentally distinct from those of a corresponding microcavity in ordinary vacuum. At high pump intensities and for large discontinuities in the photon density of states between Mollow spectral components of atomic resonance fluorescence, the emitted intensity originating from the elastic spectral component increases with the intensity of the pump and the elastic component dominates the spectrum. In the case of a vanishing photon density of states in the spectral range surrounding the lower Mollow sideband and no dipolar dephasing, the cavity spectrum is elastic.

DOI: 10.1103/PhysRevA.74.063828 PACS number(s): 42.55.Tv, 42.50.Ct, 42.50.Ar

I. INTRODUCTION

A microlaser with a single atom or a quantum dot interacting with the quantized field of a high-Q microcavity represents an important tool for the investigation of novel quantum electrodynamic effects. In free space, in the optical domain, high-Q optical cavities have enabled the investigation of the vacuum Rabi splitting [1], photon antibunching [2], and conditional phase shifts for quantum logic gates [3]. Recently, a one-atom laser consisting of a single atom trapped inside a high-quality factor microcavity and externally pumped has been realized [4]. It was shown that the characteristics of the pumped atom-cavity system are qualitatively different from those of the familiar many-atom lasers. In particular, this one-atom laser produces nonclassical light and can act as an efficient source for deterministic generation of single-photon pulses [5].

On the other hand, the unique properties of photonic crystals [6,7], engineered periodic dielectric materials, led to novel optical phenomena, such as photon-atom bound states [8], fractionalized single-atom inversion [9], optical bistability and switching in multiatom systems [10], or coherent control of spontaneous emission through quantum interference [11]. One of the key features that distinguishes the photonic radiation reservoir associated with a photonic crystal from its free-space counterpart is that the photonic density of states (DOS) within or near a photonic band gap (PBG) can nearly vanish or exhibit discontinuous changes as a function of frequency with appropriate engineering. Also, novel phenomena in quantum electrodynamics in photonic crystals stem from the possibility of simultaneously realizing extremely small microcavity-mode volumes and very high cavity Q factors. For instance, in a two-dimensional (2D) photonic crystal, a microlaser with a cavity volume of 0.03 μm^3 has already been demonstrated [12]. Within a 3D PBG, with complete light localization [13,7], there is no fundamental upper bound to the microcavity Q factor. Recently, remarkable experimental progress in coupling single quantum dots to a photonic crystal microcavity has been made. Significant modifications of the spontaneous emission and photon antibunching have been demonstrated for single emitters embedded in a photonic crystal microcavity [14]. Also, deterministic coupling of a single quantum dot to a photonic crystal cavity has been realized [15], and a thresholdless laser operating on a single quantum dot is expected to be achieved [16]. In parallel with these experimental advances, a detailed quantum theory of a one-atom laser in an engineered PBG microchip was put forward recently [17], and novel one-atom laser features have been unveiled. In particular, strong enhancement of the cavity field relative to that of a cavity in ordinary vacuum and better coherence resulting from the radiation reservoir of the PBG microchip have been predicted.

In this paper we investigate the emission spectrum of a two-level atom coupled to a high-quality microcavity embedded within a photonic crystal and coherently pumped by a strong external field. In this study, the cavity field is tuned on resonance with the Mollow central component of atomic resonance fluorescence. Using a secular approximation [19], our model yields an analytical solution for the emission spectrum. We show that the cavity spectrum, consisting of both elastic and inelastic components, has distinct characteristics from those corresponding to a conventional cavity. In a photonic crystal, the strong enhancement of the cavity field is accompanied by a narrowing of the emission spectrum. Also, the elastic spectral component is shown to be dominant at large values of the pump intensity, in contrast to the case of a conventional cavity in ordinary vacuum, where the inelastic spectral component dominates the cavity spectrum.

II. MODEL

We consider a single two-level atom driven by a coherent external laser field and coupled to a high-Q microcavity engineered within a photonic crystal. Such a system can be realized, for instance, by embedding a quantum dot in a dielectric microcavity (defect) placed within a two-mode waveguide channel in a 2D PBG microchip [17]. One mode of the waveguide channel is engineered to produce a large

discontinuity in the local photon density of states near the atom, and another mode is used to propagate the pump beam. By suitable engineering, it is possible to realize a strong coupling of the quantum dot to both the pumping waveguide mode and the high-Q cavity mode [17]. The atom has excited state $|2\rangle$, ground state $|1\rangle$, and transition frequency ω_a. The coupling constant between the atomic transition and the microcavity mode is denoted by g. The atom is driven near resonance by a coherent external field at a frequency ω_L and Rabi frequency (intensity) ε. For simplicity, we treat the driving external field classically and work in the interaction picture. The excited atomic system decays by spontaneous emission to the modes of the radiation reservoir associated with the engineered photonic crystal. The dephasing of the atomic system, which may arise from scattering of phonons of the host crystal on the atom embedded in the solid part of the dielectric material, takes place at a rate γ_p, and the cavity field is damped at the rate κ, caused by the extraneous coupling of the cavity mode to the engineered waveguide modes or possible leakage of light from the microcavity in the vertical direction. The master equation for the density operator χ of the atom-cavity field-reservoir system has the form

$$\frac{\partial}{\partial t}\chi = \frac{1}{i\hbar}[H,\chi] + \frac{\kappa}{2}[2a\chi a^{\dagger} - a^{\dagger}a\chi - \chi a^{\dagger}a] + \gamma_p(2\sigma_3\chi\sigma_3 - \chi), \tag{2.1}$$

where $H=H_0+H_1$ is the Hamiltonian of the system in the interaction picture. Here,

$$H_0 = \hbar\,\Delta_c a^{\dagger}a + \frac{1}{2}\hbar\,\Delta_a\sigma_3 + \hbar\,\varepsilon(\sigma_{12}+\sigma_{21}) + \hbar\sum_{\lambda}\Delta_{\lambda}a_{\lambda}^{\dagger}a_{\lambda}, \tag{2.2}$$

and the individual terms describe the unperturbed microcavity field, the atomic system, the interaction between the atomic system and the monochromatic pump laser field, and the remainder of the radiation reservoir of the photonic crystal (responsible for the radiative decay of the atom). The interaction Hamiltonian H_1 is written as

$$H_1 = i\hbar\,g(a^{\dagger}\sigma_{12} - \sigma_{21}a) + i\hbar\sum_{\lambda} g_{\lambda}(a_{\lambda}^{\dagger}\sigma_{12} - \sigma_{21}a_{\lambda}), \tag{2.3}$$

where the individual terms describe the interaction between the atomic system and the microcavity field, and the interaction between the atomic system and the remainder of the photonic crystal radiation reservoir, respectively. Here, a and $a^{\dagger}$ are the cavity-mode annihilation and creation operators. σ_{ij} are the bare atomic operators, $\sigma_{ij}=|i\rangle\langle j|$ $(i,j=1,2)$, and $\sigma_3=\sigma_{22}-\sigma_{11}$ describes the bare atomic inversion. The coupling constant between the atom and the cavity mode is given by $g=(\omega_a d_{21}/\hbar)(\hbar/2\epsilon_0\omega_c V)^{1/2}\mathbf{e}\cdot\mathbf{u}_d$, where d_{12} and $\mathbf{u}_d$ are the absolute value and the unit vector of the atomic dipole moment, V is the volume of the cavity mode, $\mathbf{e}$ is the polarization mode of the cavity radiation field, and ϵ_0 is the Coulomb constant. In the optical regime, dipole moments of $d_{21}\approx 10^{-29}$ C m, and a microcavity-mode volume of $V\approx(1\ \mu\text{m})^3$ yield a coupling constant of the order $g\approx 10^{-5}\omega_a$. a_{λ} and $a_{\lambda}^{\dagger}$ are the photonic crystal radiation reservoir annihilation and creation operators. $\Delta_a=\omega_a-\omega_L$, $\Delta_c=\omega_c-\omega_L$, and $\Delta_{\lambda}=\omega_{\lambda}-\omega_L$, are the detuning of the atomic resonance frequency, of the cavity-mode frequency ω_c, and of the frequency ω_{λ} of a mode λ of the photonic crystal radiation reservoir from the pump laser frequency. g_{λ} is the coupling constant between the atom and the mode λ of the radiation field of the photonic reservoir. The relevant frequencies for this study and their relative position are presented in Fig. 1.

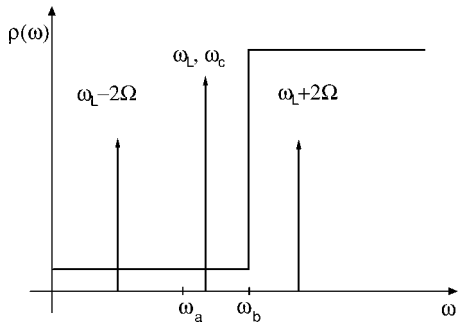

FIG. 1. The relative position of the relevant frequencies considered in our study. ω_a, ω_L, and ω_c are the atomic transition frequency, the frequency of the coherent pump field, and the microcavity field frequency, respectively. $\omega\pm 2\Omega$ describe the sideband components of the Mollow spectrum (Ω is the generalized Rabi frequency), and ω_b is the photonic DOS band edge frequency.

The master equation (2.1) is written in the basis $\{|i\rangle\}_{i=1,2}$ of bare atomic states. We introduce instead the dressed states $\{|\tilde{i}\rangle\}_{i=1,2}$ [10,18], which are the states of the atomic system dressed by the driving field,

$$|\tilde{1}\rangle = c|1\rangle - s|2\rangle, \tag{2.4}$$

$$|\tilde{2}\rangle = s|1\rangle - c|2\rangle. \tag{2.5}$$

Here, $c\equiv\cos(\phi)$, $s\equiv\sin(\phi)$, with ϕ the rotation angle that belongs in the interval $[0,\ \pi]$ and is defined by

$$\cos^2\phi = \frac{1}{2}\left(1+\frac{\Delta_a}{\Omega}\right), \tag{2.6}$$

where

$$\Omega = (4\epsilon^2 + \Delta_a^2)^{1/2} \tag{2.7}$$

is the generalized Rabi frequency.

In the dressed-state basis, the bare-state atomic operators σ_{ij} in the system Hamiltonian H are replaced by the dressed-state atomic operators $R_{ij}=|\tilde{i}\rangle\langle\tilde{j}|$, according to the transformation

$$\sigma_{12} = \frac{1}{2}\sin(2\phi)R_3 - \sin^2\phi R_{21} + \cos^2\phi R_{12}, \tag{2.8a}$$

$$\sigma_{22} - \sigma_{11} = \cos(2\phi)R_3 - \sin(2\phi)(R_{12}+R_{21}). \tag{2.8b}$$

This leads to the dressed-state Hamiltonian

$$H_0 = \hbar\,\Omega R_3 + \hbar\,\Delta_c a^\dagger a + \hbar \sum_\lambda \Delta_\lambda a_\lambda^\dagger a_\lambda. \tag{2.9}$$

Further, we define the time-dependent interaction picture Hamiltonian $\tilde{H}_1(t)=U^\dagger(t)H_1U(t)$, where $U(t)=\exp(-iH_0t/\hbar)$. In this interaction picture, the interaction Hamiltonian takes the form

$$\begin{aligned} H_1 = {} & i\hbar\, g(sca^\dagger R_3 e^{i\Delta_c t} + c^2 a^\dagger R_{12} e^{i(\Delta_c - 2\Omega)} - s^2 a^\dagger R_{21} e^{i(\Delta_c + 2\Omega)}) \\ & + i\hbar \sum_\lambda g_\lambda (sca_\lambda^\dagger R_3 e^{i\Delta_\lambda t} + c^2 a_\lambda^\dagger R_{12} e^{i(\Delta_\lambda - 2\Omega)} \\ & - s^2 a_\lambda^\dagger R_{21} e^{i(\Delta_\lambda + 2\Omega)}) + \text{H.c.} \end{aligned} \tag{2.10}$$

Hereafter, we drop the tilde on the interaction picture operators, for the sake of notational simplicity.

The master equation for the reduced density operator of the system of atom plus cavity, $\rho=\mathrm{Tr}_R\chi$, in the dressed-state basis, is derived from the resulting master equation obeyed by the density operator χ [obtained from Eq. (2.1)] by tracing over the photonic crystal radiation reservoir variables [20] (an operation denoted here by Tr_R). This equation has been derived in Ref. [17] in the secular [19] and Born-Markov [20] approximations. The Born approximation assumes a weak coupling between the atomic system and the radiation reservoir of the photonic crystal, and also that changes in the photonic reservoir as a result of atom-reservoir interaction are negligible. The Markov approximation assumes a fast time scale for the decay of the reservoir correlations, which is implied in our case by the assumption that the photonic density of modes is constant over the spectral regions surrounding the dressed-state resonant frequencies. The secular approximation is based on the assumption that the driving field is strong enough that the generalized Rabi frequency Ω is much larger than the decay rates. The validity of these approximations for the case of a photonic crystal is discussed in detail in Refs. [9,21,17]. The master equation for the system of atom + cavity field is [17]

$$\begin{aligned} \frac{\partial\rho}{\partial t} = {} & g\{sc[a^\dagger R_3 e^{i\Delta_c t} - R_3 a e^{-i\Delta_c t}, \rho] + c^2[a^\dagger R_{12} e^{i(\Delta_c - 2\Omega)t} \\ & - R_{21} a e^{-i(\Delta_c - 2\Omega)t}, \rho] - s^2[a^\dagger R_{21} e^{i(\Delta_c + 2\Omega)t} \\ & - R_{12} a e^{-i(\Delta_c + 2\Omega)t}, \rho]\} + \left\{ \frac{A_0}{2}[R_3\rho R_3 - \rho] + \frac{A_-}{2}[R_{21}\rho R_{12} \right. \\ & \left. - R_{11}\rho] + \frac{A_+}{2}[R_{12}\rho R_{21} - R_{22}\rho] + \text{H.c.} \right\} + \frac{\kappa}{2}[2a\rho a^\dagger \\ & - a^\dagger a\rho - \rho a^\dagger a]. \end{aligned} \tag{2.11}$$

The first group of terms in the master equation (2.11) corresponds to the interaction between the dressed atomic system and the cavity mode, the second group of terms describes the spontaneous emission of the dressed atom into the modes of the photonic crystal radiation reservoir, and the last group of terms describes the damping of the cavity mode via cavity decay. In Eq. (2.11), $A_0=\gamma_0 s^2c^2+\gamma_p(c^2-s^2)$, $A_-=\gamma_- s^4+4\gamma_p s^2c^2$, and $A_+=\gamma_+ c^4+4\gamma_p s^2c^2$, and the spontaneous emission decay rates $\gamma_0=2\pi\Sigma_\lambda g_\lambda^2\delta(\omega_\lambda-\omega_L)$, $\gamma_-=2\pi\Sigma_\lambda g_\lambda^2\delta(\omega_\lambda-\omega_L+2\Omega)$, and $\gamma_+=2\pi\Sigma_\lambda g_\lambda^2\delta(\omega_\lambda-\omega_L-2\Omega)$ are proportional to the density of modes at the dressed-state transition frequencies ω_L and $\omega_L\pm2\Omega$. We note that, for $\gamma_0=\gamma_+=\gamma_-=\gamma$, Eq. (2.11) has the same form as for the case of a conventional cavity [22]. Within the secular approximation that we use here, the generalized Rabi frequency, Ω, is considered much larger than the decay rates γ_0, γ_+, and γ_-.

We consider the case when the cavity field is tuned on resonance with the central component of the Mollow spectrum ($\Delta_c=0$). Assuming a strong pump field ($\Omega\gg\kappa$), one can invoke the secular approximation to ignore the rapidly oscillating terms at frequencies 2Ω and 4Ω in the master equation (2.11). The master equation (2.11) reduces in this case to

$$\begin{aligned} \frac{\partial\rho}{\partial t} = {} & g_1[(a^\dagger - a)R_3, \rho] + \left\{ A_0[R_3\rho R_3 - \rho] + \frac{A_-}{2}[2R_{21}\rho R_{12} \right. \\ & \left. - R_{11}\rho - \rho R_{11}] + \frac{A_+}{2}[2R_{12}\rho R_{21} - R_{22}\rho - \rho R_{22}] \right\} \\ & + \frac{\kappa}{2}[2a\rho a^\dagger - a^\dagger a\rho - \rho a^\dagger a], \end{aligned} \tag{2.12}$$

where $g_1\equiv gcs$ is the pump-dependent "effective" coupling constant. The master equation (2.12) is employed to derive the properties of the one-atom laser in the engineered vacuum of a PBG material.

III. SPECTRUM OF THE CAVITY FIELD

In this section we investigate the spectrum of the cavity field, defined as the Fourier transform of the two-time correlation function $\langle a^\dagger(t)a\rangle_s$ of the interaction picture cavity field operators:

$$S(\omega) = 2\,\mathrm{Re}\int_0^\infty dt\, e^{i(\omega-\omega_L)t}\langle a^\dagger(t)a\rangle_s. \tag{3.1}$$

Here ω is the spectral frequency, s indicates steady-state averages, and the operators without time argument refer to their values at $t=0$.

By rewriting the cavity field operators in the form $a(t)=\langle a(t)\rangle+\delta a(t)$, where $\delta a(t)=a(t)-\langle a(t)\rangle$ describes the fluctuations about the average value and satisfy $\langle\delta a(t)\rangle=0$, one obtains that $\langle a^\dagger(t)a\rangle_s=\langle a^\dagger\rangle_s\langle a\rangle_s+\langle\delta a^\dagger(t)\,\delta a\rangle_s$, such that the cavity spectrum decomposes into a coherent (elastic) part, determined by the average value of the cavity field, and an incoherent (inelastic) part, arising from quantum fluctuations,

$$S(\omega) = S_{el}(\omega) + S_{inel}(\omega). \tag{3.2}$$

Here, the elastic spectral component $S_{el}(\omega)$ is expressed as

$$S_{el}(\omega) = 2\pi\langle a^\dagger\rangle_s\langle a\rangle_s\delta(\omega-\omega_L), \tag{3.3}$$

and the inelastic spectral component $S_{in}(\omega)$ is defined by

$$S_{inel}(\omega) = 2\,\mathrm{Re}\int_0^\infty dt\, e^{i(\omega-\omega_L)t}\langle\delta a^\dagger(t)\,\delta a\rangle_s. \tag{3.4}$$

The elastic spectral component corresponds to the elastic scattering of the pump photons by the atom into the cavity

mode, while the inelastic component is associated with atomic fluorescence and cavity decay. In practice, the elastic spectral component contributes to the measurements as a peak of finite width because of the finite spectral resolution of the detector and of the fact that the exciting field is not strictly monochromatic. As a result of the presence of the elastic component, the spectral linewidth of the cavity field can be much smaller than the cavity linewidth. Moreover, the properties of the photonic reservoir associated with the photonic crystal may contribute to a further narrowing of the emission spectrum, as we shall present below.

Generally, the two-time correlation function $\langle \delta a^\dagger(t)\delta a\rangle_s$ in the definition (3.4) of the inelastic component of the cavity spectrum may be calculated approximately using the numerical solution of the master equation (2.12), or by means of certain factorization schemes. However, our model enables an exact and simple analytical solution for the emission spectrum. From the master equation (2.12) one can derive the equations of motion for the expectation values of the atomic and cavity field operators. Using the fact that the cavity and atomic operators are time-independent Schrödinger operators, the equations of motion for their expectation values follow from the master equation (2.12). The following closed set of equations of motion for the expectation values of various operators is obtained:

$$\frac{d}{dt}\langle a\rangle = -\frac{\kappa}{2}\langle a\rangle + g_1\langle R_3\rangle, \tag{3.5a}$$

$$\frac{d}{dt}\langle R_3\rangle = -\gamma_2 - \gamma_1\langle R_3\rangle, \tag{3.5b}$$

$$\frac{d}{dt}\langle a^\dagger a\rangle = -\kappa\langle a^\dagger a\rangle + g_1\langle R_3 a^\dagger\rangle + g_1\langle R_3 a\rangle, \tag{3.5c}$$

$$\frac{d}{dt}\langle R_3 a\rangle = -(\gamma_1 + \kappa/2)\langle R_3 a\rangle + g_1 - \gamma_2\langle a\rangle, \tag{3.5d}$$

where $\gamma_{1,2}$ are defined by

$$\gamma_1 = \frac{\gamma_+ c^4 + \gamma_- s^4}{2} + 4\gamma_p s^2 c^2, \tag{3.6a}$$

$$\gamma_2 = \frac{\gamma_+ c^4 - \gamma_- s^4}{2}. \tag{3.6b}$$

For a Markovian system, like the one assumed here, one can apply the quantum regression theorem [20] to derive the two-time correlation function $\langle a^\dagger(t)a\rangle_s$. According to the quantum regression theorem, the two-time correlation functions of the system obey exactly the same dynamical law of evolution as the one-time correlation functions. We obtain

$$\frac{d}{dt}\langle a^\dagger(t)a\rangle_s = -\frac{k}{2}\langle a^\dagger(t)a\rangle_s + g_1\langle R_3(t)a\rangle_s, \tag{3.7}$$

$$\frac{d}{dt}\langle R_3(t)a\rangle_s = -\gamma_2\langle a\rangle_s - \gamma_1\langle R_3(t)a\rangle_s. \tag{3.8}$$

The initial conditions for Eqs. (3.7) and (3.8) are $\langle a^\dagger(0)a\rangle_s = \langle a^\dagger a\rangle_s$ and $\langle R_3(0)a\rangle_s = \langle R_3 a\rangle_s$, where $\langle a^\dagger a\rangle_s$ and $\langle R_3 a\rangle_s$ are the steady-state values of the single-time correlation functions $\langle a^\dagger a\rangle$ and $\langle R_3 a\rangle$. Equations (3.7) and (3.8) can be solved exactly, and the two-time correlation function $\langle \delta a^\dagger(t)\delta a\rangle_s$ can be written as

$$\langle \delta a^\dagger(t)\delta a\rangle_s = \frac{2g_1}{k-2\gamma_1}\left(\langle R_3 a\rangle_s + \frac{\gamma_2}{\gamma_1}\langle a\rangle_s\right)e^{-\gamma_1 t} + \left[\langle a^\dagger a\rangle_s - \frac{2g_1}{k-2\gamma_1}\left(\langle R_3 a\rangle_s + \frac{2\gamma_2}{k}\langle a\rangle_s\right)\right]e^{-kt/2}. \tag{3.9}$$

Here, the expectation values $\langle a\rangle_s$, $\langle a^\dagger a\rangle_s$, and $\langle R_3 a\rangle_s$ are obtained from Eqs. (3.5a), (3.5b), (3.5c), and (3.5d) as

$$\langle a\rangle_s = \langle a^\dagger\rangle_s^* = -\frac{2g_1}{\kappa}\frac{\gamma_2}{\gamma_1}, \tag{3.10}$$

$$\langle a^\dagger a\rangle_s = \frac{4g_1^2}{\kappa^2}\frac{(\kappa\gamma_1 + 2\gamma_2^2)}{\gamma_1(\kappa + 2\gamma_1)}, \tag{3.11}$$

$$\langle R_3 a\rangle_s = \frac{2g_1}{k}\frac{(\kappa\gamma_1 + 2\gamma_2^2)}{\gamma_1(\kappa + 2\gamma_1)}. \tag{3.12}$$

It is apparent from Eq. (3.9) and the definition (3.4) that the inelastic emission spectrum contains two Lorentzian components with the linewidths $2\gamma_1$ and k, respectively. Using the expressions (3.10)–(3.12), the two-time correlation function (3.9) can be written as

$$\langle \delta a^\dagger(t)\delta a\rangle_s = (\gamma_1^2 - \gamma_2^2)\frac{g_1^2}{\gamma_1[(k/2)^2 - \gamma_1^2]}\left(\frac{e^{-\gamma_1 t}}{\gamma_1} - \frac{e^{-kt/2t}}{k/2}\right), \tag{3.13}$$

and the cavity spectral components defined by (3.3) and (3.4) take the forms

$$S_{el}(\omega) = \frac{8\pi g_1^2}{k^2}\frac{\gamma_2^2}{\gamma_1^2}\delta(\omega - \omega_L) \tag{3.14}$$

and

$$S_{inel}(\omega) = (\gamma_1^2 - \gamma_2^2)\frac{2g_1^2}{\gamma_1}\frac{1}{[(\omega-\omega_L)^2 + \gamma_1^2][(\omega-\omega_L)^2 + (k/2)^2]}. \tag{3.15}$$

We first note that, in general, both the elastic and inelastic components of the emission spectrum are present. This is a direct consequence of the fact that $\gamma_1^2 > \gamma_2^2$. In the case of vanishing mode density on the lower Mollow sideband ($\gamma_- = 0$, which corresponds to a full photonic band gap) and no dipolar dephasing ($\gamma_p = 0$), $\gamma_1 = \gamma_2$ and the spectrum of the cavity field consists only of the elastic component. In this case the atom scatters photons only elastically, similar to a perfect classical scatterer [23]. This is in contrast to the case of a conventional cavity in vacuum, when the inelastic com-

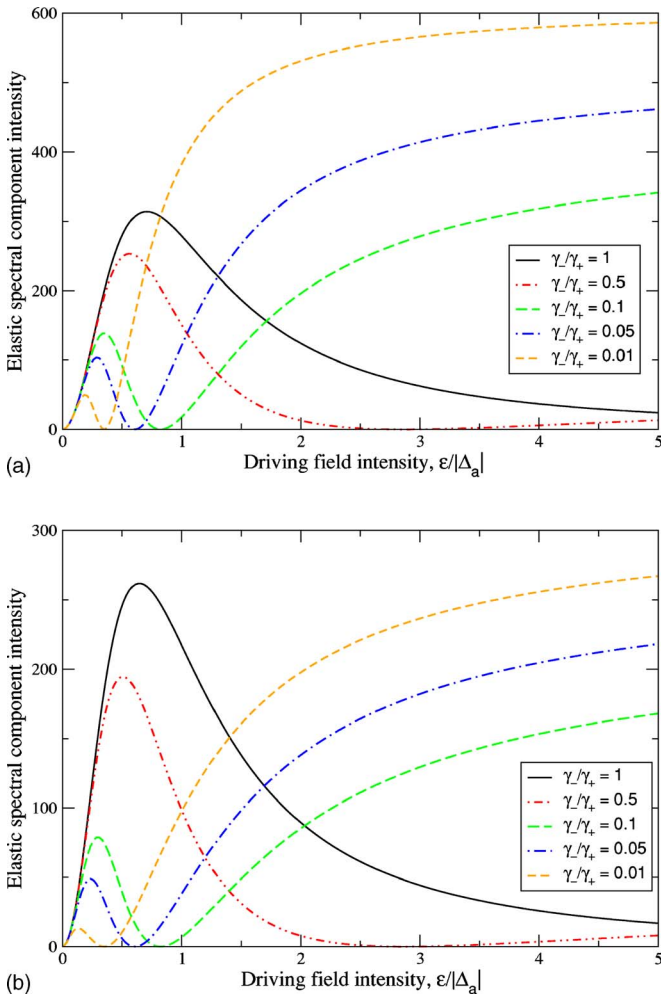

FIG. 2. (Color online) The emitted intensity originating from the elastic component of the emission spectrum as a function of the scaled driving field Rabi frequency $\varepsilon/|\Delta_a|$ for negative detuning between the atomic resonant frequency and the driving field frequency, $\Delta_a<0$, and for various values of the jump in the photonic DOS, γ_-/γ_+, (a) in the absence of dipolar dephasing ($\gamma_p=0$) and (b) in the presence of dipolar dephasing, $\gamma_p=0.05\gamma_+$. We have set $\kappa=0.1\gamma_+$ and $g=10\kappa$ in the calculations.

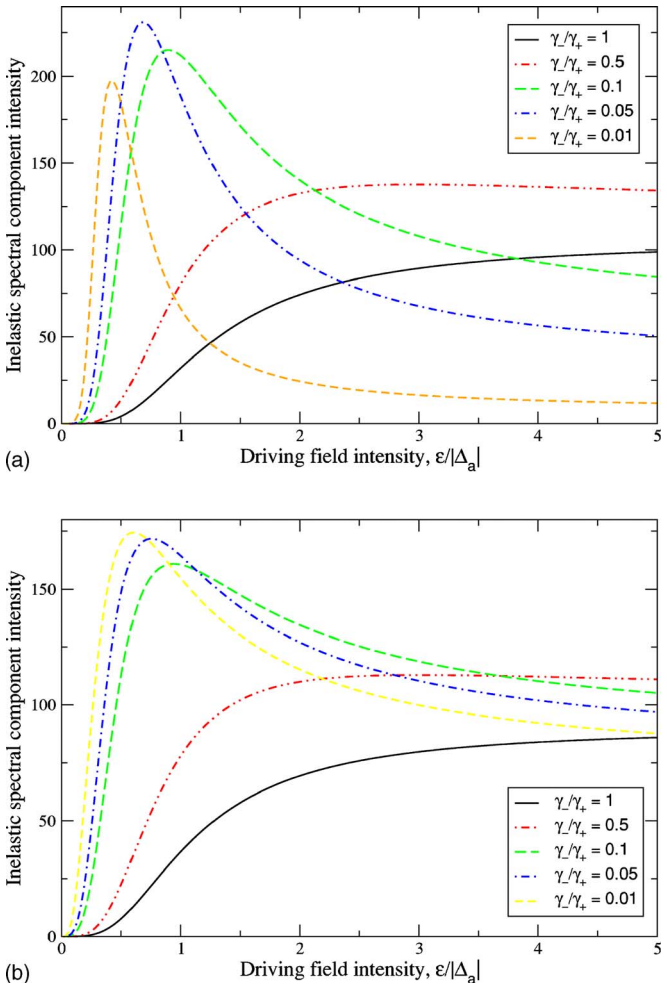

FIG. 3. (Color online) The emitted intensity originating from the inelastic component of the emission spectrum as a function of the scaled driving field Rabi frequency $\varepsilon/|\Delta_a|$ for negative detuning between the atomic resonant frequency and the driving field frequency, $\Delta_a<0$, and for various values of the jump in the photonic DOS, γ_-/γ_+, (a) in the absence of dipolar dephasing ($\gamma_p=0$) and (b) in the presence of dipolar dephasing, $\gamma_p=0.05\gamma_+$. We have set $\kappa=0.1\gamma_+$ and $g=10\kappa$ in the calculations.

ponent is always present. Thus, the measured cavity spectrum is the narrowest in the case when the microcavity resonance occurs in a photonic band gap. This effect is accompanied by strong emission enhancement, Poissonian photon statistics, and quadrature coherence of the cavity field, which have already been predicted for the full photonic band gap case [17].

The spectrum of the cavity field has distinct characteristics from those corresponding to a conventional cavity in ordinary vacuum. This can be inferred from Figs. 2 and 3, where we plot the integrated elastic and inelastic spectral components as a function of the driving field intensity, for various values of the discontinuity in the photonic density of states, γ_-/γ_+, ranging from the case of a large discontinuity in the photonic density of states, $\gamma_-/\gamma_+=0.01$, to the case of a cavity in free space, $\gamma_-/\gamma_+=1$. We consider negative detuning between the atomic resonant frequency and the driving field frequency, $\Delta_a<0$, and a cavity decay rate given by $\kappa/\gamma_+=0.1$. We obtain that at larger values of the driving field intensity (but corresponding to nanowatt pump power [24]), the elastic spectral component of the cavity in a photonic crystal increases with the driving field intensity and dominates the emission spectrum, being also strongly enhanced in photonic structures presenting large jumps in the photonic density of states. This is different from the case of a cavity in free space, when the elastic spectral component decreases with increase of the driving field intensity and the inelastic component dominates the emission spectrum at larger values of the pump field intensity. Equivalently, the inelastic spectral component of the cavity in a photonic crystal decreases with increase of the driving field intensity, as opposed to the case of a conventional cavity in free space, where the inelastic component increases with increase of the pumping field intensity. The dephasing processes have a deleterious effect on the light generation, lowering the number of photons in the cavity mode relative to the case when no dipolar dephas-

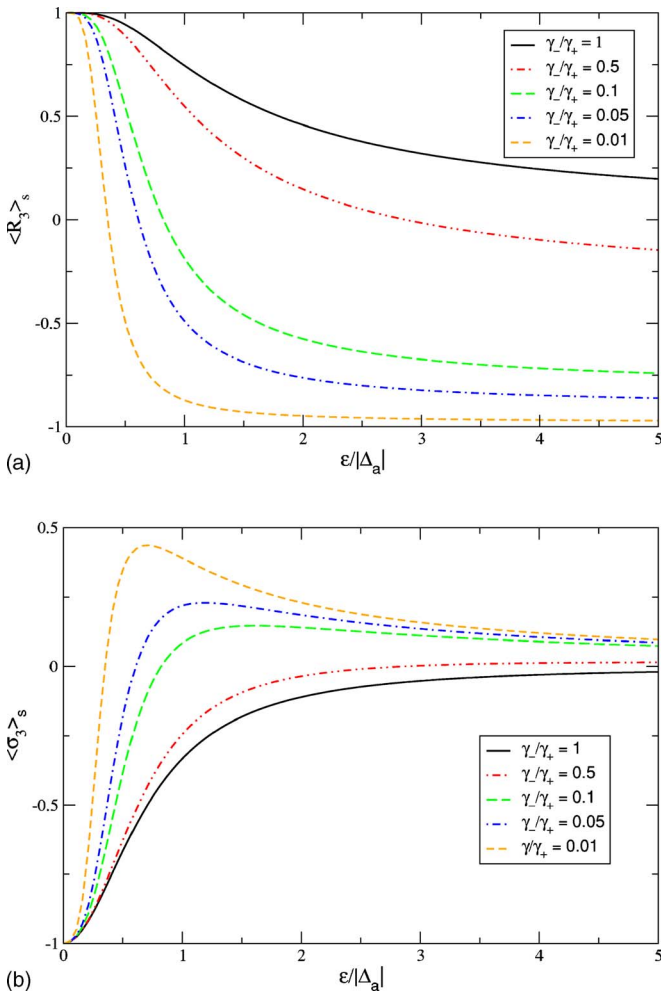

FIG. 4. (Color online) The steady-state (a) dressed and (b) bare atomic population inversion, $\langle R_3\rangle_s$ and $\langle \sigma_3\rangle_s$ as functions of the scaled Rabi driving field frequency $\varepsilon/|\Delta_a|$ for negative detuning between the atomic resonant frequency and the driving field frequency, $\Delta_a<0$, and for various values of the magnitude of the jump in the photonic density of states, γ_-/γ_+.

ing is present, but the general spectral characteristics are preserved.

To understand these characteristics, recall first that the elastic spectral component is determined by the average cavity field, determined, in turn, by the dressed atomic population inversion [according to Eq. (3.5a)]. The resulting dependence of the elastic spectral component on the dressed atomic population inversion can be expressed in the form

$$S_{el}(\omega) = \frac{8\pi g_1^2}{k^2}\langle R_3\rangle_s^2 \delta(\omega-\omega_L). \tag{3.16}$$

In Fig. 4 we plot the atomic population inversion as a function of the driving field intensity, for various values of the discontinuity in the photonic density of states. We note that, for photonic structures characterized by small jumps in the photonic DOS and in free space, the dressed atomic population inversions $\langle R_3\rangle_s$ approach zero at large values of the driving field. Thus, the source for the cavity field is very small in this case, and the field amplitude decreases in time and reaches a very small steady-state value, leading to reduced light generation into the elastic spectral component. On the other hand, large values of the discontinuity in the photonic density of states of the radiation reservoir facilitate an entirely different behavior of the atomic system. In this case, at large driving field intensities, the dressed atomic system is trapped in the dressed ground state $|\tilde{1}\rangle$, and the dressed-state atomic population inversion achieves values close to -1. This is accompanied by positive bare atomic population inversion. As a result, the steady-state cavity field amplitude, and implicitly the elastic spectral component, attain finite values that increase with increase of the pump intensity and the jump in the photonic density of states. The possibility of inverting a two-level system in photonic crystals represents the basis of a series of novel effects in quantum optics and has been explained in detail in Ref. [25]. It results from the very different spontaneous emission rates experienced by the Mollow spectral components in photonic crystals. More specifically, for large jumps in the photonic density of states and large values of the driving field intensity, the rate of depopulation of the atomic dressed excited state $|\tilde{2}\rangle$ state, A_+, exceeds that of population, A_-, and the atomic system remains in the dressed ground state $|\tilde{1}\rangle$ (mostly comprised of the excited bare state $|2\rangle$). This is in contrast to the free space case, where always $A_->A_+$ (for negative atom-field detunings), and the atomic system is trapped in the excited dressed state, $|\tilde{2}\rangle$ (mostly comprised of the bare ground state $|1\rangle$).

From the analytical expressions (3.3) and (3.4), it follows that the elastic spectral component as a function of the intensity of the driving field exhibits a local minimum where it vanishes, concomitant with the inelastic component exhibiting a local maximum. This occurs at the pump intensity that causes the atomic inversion ($\langle R_3\rangle_s=0$). In addition, other interesting single-atom laser features, such as a maximal quantum degree of second-order coherence, corresponding to the tendency to emit photons in pairs, have been predicted at this inversion threshold [17].

The linewidth of the inelastic spectral component (full width at half maximum) is calculated from Eq. (3.4) as

$$\Delta\omega = \left(\frac{\left[(k^2+4\gamma_1^2)^2+16\gamma_1^2k^2\right]^{1/2}-(k^2+4\gamma_1^2)}{2}\right)^{1/2}. \tag{3.17}$$

In Fig. 5, we plot the inelastic spectral linewidth $\Delta\omega$ as a function of Rabi driving field frequency ε in the case when no dipolar dephasing is present in the system, for various values of the magnitude of the discontinuity in the photonic density of states, γ_-/γ_+. We obtain that for all values of the driving field intensity the emission spectral linewidth is reduced in photonic structures presenting large jumps in the photonic density of states, relative to that of a conventional cavity in free space.

In Fig. 6, we plot the spectral linewidth as a function of the cavity decay rate at the inversion threshold, when only the inelastic component is present ($\gamma_2=0$). This occurs for a

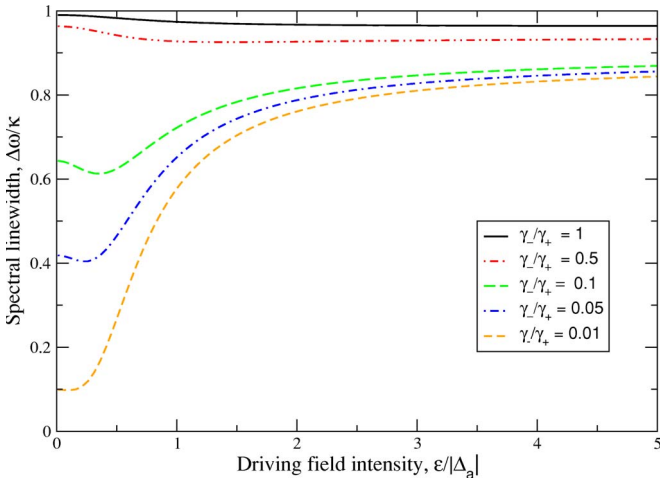

FIG. 5. (Color online) The inelastic spectral linewidth $\Delta\omega$ as a function of Rabi driving field frequency $\varepsilon/|\Delta_a|$ in the absence of dipolar dephasing, for negative detuning between the atomic resonant frequency and the driving field frequency, $\Delta_a<0$, and for various values of the magnitude of the jump in the photonic density of states, γ_-/γ_+. We have set $\kappa=0.1\gamma_+$ and $\gamma_p=0$ in the calculations.

driving field intensity given by $\varepsilon/|\Delta_a|=(\gamma_-/\gamma_+)^{1/4}/[1-(\gamma_-/\gamma_+)^{1/2}]$, which decreases with increase of the discontinuity in the photonic density of states, γ_-/γ_+. Clearly, the emission spectral linewidth is strongly reduced for larger jumps in the photonic density of states for all values of the cavity decay rate, even when additional dephasing is introduced in the system.

In general, both the elastic and inelastic spectral components contribute to the measurements, and the dominance of the elastic component in the emission spectrum together with the narrowing of the inelastic spectrum strongly reduce the total emission linewidth in the case when emission occurs in a photonic crystal. This can be seen in Fig. 7 which presents the linewidth of the measured cavity spectrum obtained by a convolution of the expression (3.2) with an instrumental profile, considered, for simplicity, of Lorentzian shape with a width $\delta=0.005\gamma_+$. We obtain a strong reduction of the emission spectral linewidth for large values of the discontinuity in the photonic density of states and at reasonably large driving field intensities. This is accompanied by a strong enhancement of the emitted intensity, as shown in Fig. 8, where the scaled steady-state emitted intensity is plotted as a function of Rabi driving field frequency, for various values of the magnitude of the discontinuity in the photonic density of states. We note that, for smaller values of the driving field intensity, the spectrum is narrower for a cavity in free space. However, in this case, the number of photons in the cavity field is smaller compared with that in a cavity in a photonic crystal at slightly larger values of the driving field intensity. The local maximum presented by the spectral linewidth as a function of the driving field intensity originates from the vanishing of the elastic spectral component at the inversion threshold, when only the broader inelastic component contributes to the cavity spectrum.

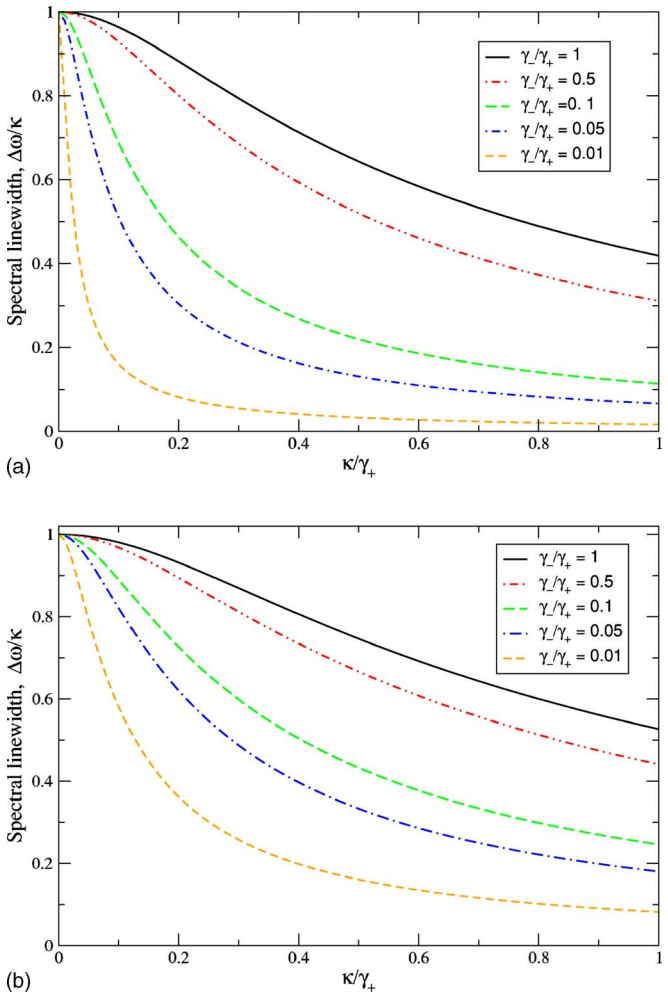

FIG. 6. (Color online) The spectral linewidth $\Delta\omega$ as a function of the scaled cavity decay rate κ/γ_+ at the inversion threshold, for negative detuning between the atomic resonant frequency and the driving field frequency, $\Delta_a<0$, and for various values of the jump in the photonic DOS, γ_-/γ_+, (a) in the absence of dipolar dephasing ($\gamma_p=0$) and (b) in the presence of dipolar dephasing, $\gamma_p=0.05\gamma_+$.

IV. CONCLUSIONS

We have studied the emission spectrum of a one-atom laser with coherent pumping in photonic crystals. We have considered the case of the cavity frequency tuned on resonance with the Mollow central component of the atomic resonance fluorescence spectrum. We have shown that the cavity spectrum consists of an elastic component, corresponding to the elastic scattering of pump photons by the atom into the cavity mode, and an inelastic component, associated with fluorescence and cavity decay. In the limit of strong pumping, we have an derived an analytical expression for the cavity spectrum. Novel characteristics of the one-atom laser spectrum are facilitated by the photonic crystals. We have shown that for a microcavity embedded into a photonic crystal, the elastic spectral component increases with the pump field intensity and dominates the spectrum at large values of the pump field. This is fundamentally different from the case of a microcavity in ordinary vacuum, where the inelastic spectral component dominates the spectrum at

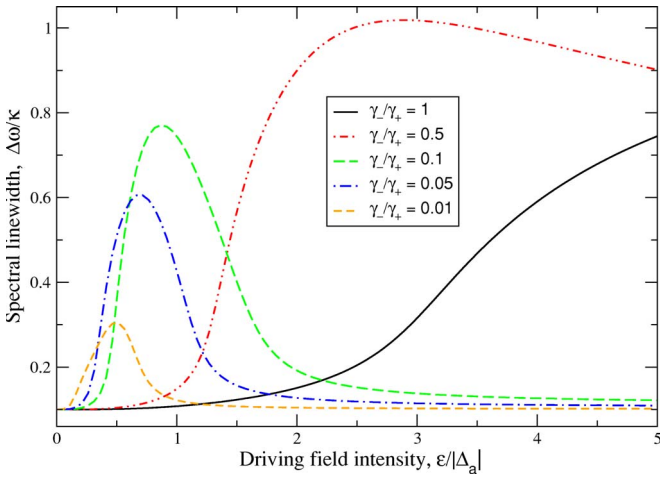

FIG. 7. (Color online) The linewidth of the measured cavity spectrum as a function of the scaled driving field Rabi frequency $\varepsilon/|\Delta_a|$ for negative detuning between the atomic resonant frequency and the driving field frequency, $\Delta_a<0$, and for various values of the jump in the photonic DOS, γ_-/γ_+. We have set $\kappa=0.1\gamma_+$ and $\gamma_p=0$ in the calculations.

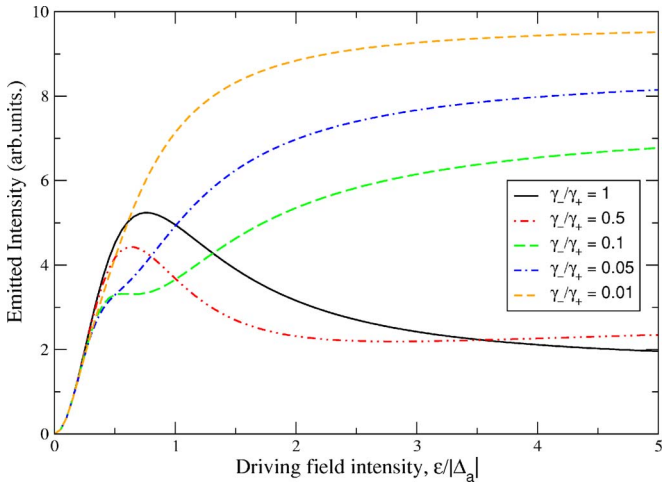

FIG. 8. (Color online) The steady-state cavity field intensity as a function of the scaled driving field Rabi frequency $\varepsilon/|\Delta_a|$ in the absence of dipolar dephasing, for negative detuning between the atomic resonant frequency and the driving field frequency, $\Delta_a<0$, and for various values of the jump in the photonic DOS, γ_-/γ_+. We have set $\kappa=0.1\gamma_+$ and $g=10\kappa$ in the calculations.

large values of the pump field. We have argued that these distinguishable features of the cavity spectrum are a direct consequence of the possibility of inverting a two-level system in photonic crystals, resulted from the discontinuous changes with frequency of the photonic density of states. We have shown that for a photonic density of states of the photonic radiation reservoir presenting a large discontinuity, the fluorescent intensity emerging from the cavity is strongly enhanced and spectrally narrower relative to the corresponding cavity in a free-space reservoir. The spectral narrowing of the cavity field in a photonic crystal is caused by the strong dominance of the elastic spectral component over the inelastic component as well as by the decrease of the fluorescence rate. Our study suggests that in order for these characteristics to be attained, a discontinuity of the photonic density of states by a factor of 100 is enough. Ultimately, if the microcavity resonance occurs in a full photonic band gap, the laser spectrum consists only of an elastic component.

ACKNOWLEDGMENTS

This work was performed at the Jet Propulsion Laboratory, California Institute of Technology under contract with the National Aeronautics and Space Administration (NASA). The author acknowledges support from the National Research Council and NASA, Code S.

[1] M. G. Raizen, R. J. Thompson, R. J. Brecha, H. J. Kimble, and H. J. Carmichael, Phys. Rev. Lett. **63**, 240 (1989).
[2] G. Rempe, R. J. Thompson, R. J. Brecha, W. D. Lee, and H. J. Kimble, Phys. Rev. Lett. **67**, 1727 (1991).
[3] Q. A. Turchette, C. J. Hood, W. Lange, H. Mabuchi, and H. J. Kimble, Phys. Rev. Lett. **75**, 4710 (1995)
[4] J. McKeever, A. Boca, A. D. Boozer, J. R. Buck, and H. J. Kimble, Nature (London) **425**, 268 (2003).
[5] J. McKeever *et al.*, Science **303**, 1992 (2004).
[6] E. Yablonovitch, Phys. Rev. Lett. **58**, 2059 (1987).
[7] S. John, Phys. Rev. Lett. **58**, 2486 (1987).
[8] S. John and J. Wang, Phys. Rev. Lett. **64**, 2418 (1990).
[9] S. John and Tran Quang, Phys. Rev. A **50**, 1764 (1994).
[10] S. John and Tran Quang, Phys. Rev. Lett. **78**, 1888 (1997); S. John and M. Florescu, J. Opt. A, Pure Appl. Opt. **3**, S103 (2001).
[11] Trang Quang, M. Woldeyohannes, S. John, and G. S. Agarwal, Phys. Rev. Lett. **79**, 5238 (1997); S. Y. Zhu, H. Chen, and Hu Huang, *ibid.* **79**, 205 (1997); D. G. Angelakis, E. Paspalakis, and P. L. Knight, Phys. Rev. A **64**, 013801 (2001); Y. V. Rostovtsev, A. B. Matsko, and M. O. Scully, *ibid.* **57**, 4919 (1998).
[12] O. Painter *et al.*, Science **284**, 1819 (1999).
[13] Sajeev John, Phys. Rev. Lett. **53**, 2169 (1984).
[14] Dirk Englund *et al.*, Phys. Rev. Lett. **95**, 013904 (2005).
[15] Antonio Badolato *et al.*, Science **308**, 1158 (2005).
[16] S. Strauf *et al.*, Phys. Rev. Lett. **96**, 127404 (2006).
[17] Lucia Florescu, Sajeev John, Tran Quang, and Rongzhou Wang, Phys. Rev. A **69**, 013816 (2004).
[18] Tran Quang and H. Freedhoff, Phys. Rev. A **47**, 2285 (1993).
[19] G. S. Agarwal, L. M. Narducci, Da Hsuan Feng, and R. Gilmore, Phys. Rev. Lett. **42**, 1260 (1978).
[20] H. J. Carmichael, *Statistical Methods in Quantum Optics 1* (Springer-Verlag, Berlin, 1999).
[21] M. Florescu and S. John, Phys. Rev. A **64**, 033801 (2001).
[22] Trang Quang and H. Freedhoff, Phys. Rev. A **47**, 2285 (1993); H. Freedhoff and Trang Quang, Phys. Rev. Lett. **72**, 474 (1994).

[23] T. W. Mosseberg and M. Lewenstein, J. Opt. Soc. Am. B **10**, 340 (1993).

[24] For frequency detunings of the order $\Delta_a \approx 10^8$ s^{-1}, the electric field amplitudes E used in our calculations are of the order of a few kV/m. On the other hand, the intensity of an electromagnetic wave is the time average over the detector response time of the Poynting vector, describing the rate of flow of electromagnetic energy. For a plane wave, the intensity I and amplitude E of the electric field are related to each other by $I\,(W/m^2) \approx 1.33 \times 10^{-3} |E\,(\mathrm{V/m})|^2$. Thus, an electric field amplitude $E \approx 10^3$ V/m, gives an intensity $I \approx 10^3$ W/m^2. For a waveguide channel with cross-sectional area on the scale of (micrometer)^2, this corresponds to a net power of about 1 nW.

[25] Marian Florescu and Sajeev John, Phys. Rev. A **69**, 053810 (2004).